On-Demand Coherent Perfect Absorption in Complex Scattering Systems: Time Delay Divergence and Enhanced Sensitivity to Perturbations

Philipp del Hougne, K. Brahima Yeo, Philippe Besnier, Matthieu Davy

On-demand coherent perfect absorption in complex scattering systems: time delay divergence and enhanced sensitivity to perturbations

Philipp del Hougne K. Brahima Yeo Philippe Besnier Matthieu Davy

Dr. P. del Hougne, K. Brahima Yeo, Dr. Philippe Besnier, Dr. M. Davy
Univ Rennes, INSA Rennes, CNRS, IETR - UMR 6164, F-35000, Rennes, France

Keywords: *Disorder, Wavefront Shaping, Coherent Perfect Absorption, Programmable Metamaterial, CPA Sensor*

Non-Hermitian photonic systems capable of perfectly absorbing incident radiation recently attracted much attention both because fundamentally they correspond to an exotic scattering phenomenon (a real-valued scattering matrix zero) and because their extreme sensitivity holds great technological promise. The sharp reflection dip is a hallmark feature underlying many envisioned applications in precision sensing, secure communication and wave filtering. However, a rigorous link between the underlying scattering anomaly and the sensitivity of the system to a perturbation is still missing. Here, a theoretical description in complex scattering systems is developed which quantitatively explains the shape of the reflection dip. It is furthermore demonstrated that coherent perfect absorption (CPA) is associated with a phase singularity and that the sign of the diverging time delay is related to the mismatch between excitation rate and intrinsic decay rate. The theoretical predictions are confirmed in experiments based on a three-dimensional chaotic cavity excited by eight channels. Rather than relying on operation frequency and attenuation inside the system to be two free parameters, "on-demand" CPA is achieved at an arbitrary frequency by tweaking the chaotic cavity's scattering properties with programmable meta-atom inclusions. Finally, the optimal sensitivity of the CPA condition to minute perturbations of the system is proven theoretically and verified experimentally.

1 Introduction

The scattering of waves as they interact with matter is the basis of countless experimental methods, a prominent example being imaging. Recently, many exotic scattering phenomena such as perfect absorption, exceptional points or bound states in the continuum have been extensively studied due to their disruptive potential in areas such as sensing and computing; fundamentally, they can be understood in terms of analytical properties of the associated scattering matrix [1]. Indeed, any wave scattering process is fully characterized by the distribution of poles and zeros of the scattering matrix in the complex frequency plane [2, 1]. Poles and zeros are spectral singularities associated with outgoing and incoming boundary conditions, respectively. By including the appropriate amount of gain in the system, a pole can be pulled up onto the real frequency axis: the scattering matrix will have an infinite eigenvalue and lasing occurs. Conversely, by including the appropriate amount of loss, a zero can be pulled down onto the real frequency axis, resulting in a zero eigenvalue of the scattering matrix and coherent perfect absorption (CPA) [3, 4]. Incident radiation corresponding to the eigenvector associated with the zero eigenvalue will be perfectly absorbed. CPA can be interpreted as a generalization of the critical coupling condition [5] and can be understood as the time reverse operation of a laser (i.e. as an "anti-laser") at the lasing threshold (before the appearance of nonlinear saturation effects) [6, 7]. The generality of these concepts implies that they also apply to random scattering media. Indeed, a "random laser" resonantly enhances light by multiple scattering inside a disordered medium [8, 9]. Recently, the feasibility of realizing CPA in random scattering media and chaotic cavities has been studied theoretically and demonstrated experimentally [10, 11, 12, 13], overcoming the immense difficulty of balancing excitation and decay rate of a random system.

A hallmark signature of a system with a scattering matrix zero on the real frequency axis is a very pronounced dip of the energy reflected off the system as a function of frequency or any other local or global system parameter, evidencing an extreme sensitivity to tiny perturbations. This feature is at the heart of the concept's technological relevance: for regular systems, it was, for instance, leveraged to demonstrate coherent modulation of light with light, i.e. without any non-linearity [14, 15, 16]; for randomly scattering systems, the extreme sensitivity is the basic ingredient of a recently demonstrated physically secure wireless communication scheme [17] as well as of envisioned precision-sensing applications [13, 17].

Intuitively, one may explain this extreme sensitivity with the fact that the incident radiation is trapped for an infinite time [3] when a real-valued scattering matrix zero is accessed: the longer the wave's lifetime inside a chaotic system, the more likely it is that its evolution is impacted even by a tiny perturbation. Nonetheless, a rigorous explanation of the physical origins of this extreme sensitivity and its link to the underlying scattering anomaly is to date missing.
In our work, we fill this gap by studying the time delay of waves at the CPA condition inside a random medium. Our theoretical model quantitatively explains the shape of the reflection dip and relates the sign of the diverging time delay to the difference between the system's excitation and decay rate. We further analytically demonstrate the CPA condition's optimal sensitivity to minute perturbations, irrespective of their location inside a chaotic system. Our theoretical findings are corroborated with random matrix simulations as well as experiments in the microwave domain involving a chaotic cavity. To facilitate accessing a real-valued zero experimentally, we follow (and generalize) an idea introduced in Ref. [17]: we tune our disordered system's scattering properties with programmable meta-atom inclusions to a state in which a zero of the scattering matrix hits the horizontal axis. This procedure enables the "on-demand" observation of a CPA condition at any desired frequency and without reliance on attenuation being dominated by a localized and tunable loss center. Our versatile setup furthermore enables a statistical study of perturbation strengths in the cases of coherent excitation of the system with an unoptimized wavefront or the CPA wavefront, revealing that the latter enables sensing the perturbation strength (for sufficiently small perturbations) whereas the former cannot discriminate between different perturber strengths. Our results pave the way for sensors with optimal sensitivity to minute perturbations of disordered matter such as tiny intrusions, defaults, changes in temperature or concentration.

2 Theoretical Model of Time Delays in Random CPA

2.1 Dip in Frequency-Dependent Reflection Coefficient

The wave-matter interaction in a complex scattering system is fully characterized by the system's scattering matrix $S(\omega)$ which relates an incoming field ψ_{in} to the corresponding outgoing field ψ_{out} via $\psi_{out} = S(\omega)\psi_{in}$. In a system without any absorption or loss, $S(\omega)$ is unitary and its zeros ($z_m = \omega_m + i\Gamma_m/2$) and poles ($\omega_m = \omega_m - i\Gamma_m/2$) are symmetrically placed in the upper and lower half of the complex frequency plane, respectively. ω_m and Γ_m denote central frequency and linewidth of the system's mth resonance. In non-Hermitian systems, the presence of attenuation (or gain) Γ_a moves the zeros in the complex plane: $z_m = \omega_m + i(\Gamma_m - \Gamma_a)/2$. Because in our subsequent experiments losses are not spatially localized but of uniform nature (specifically, they are approximately uniformly spread across the boundaries of the scattering enclosure), we assume in this theory section that there are no significant mechanisms of localized loss. When attenuation losses exactly balance dissipation through the channels for a given zero (labelled with the subscript n in the following), that is $\Gamma_a = \Gamma_n$, the zero crosses the real frequency axis such that $z_n = \omega_n$. Then, $S(\omega_n)$ has a zero eigenvalue such that the corresponding eigenvector ψ_{CPA} satisfies $S(\omega_n)\psi_{CPA} = 0$ and the multi-channel reflection coefficient $R(\omega_n) = \|\psi_{out}\|^2$ vanishes: $R(\omega_n) \to 0$. The vanishing reflection at the CPA condition suggests that the wave is infinitely trapped in the medium which we expect to translate into a diverging time delay. To rigorously investigate this hallmark property for CPA in a complex scattering system, we avail ourselves of a non-perturbative effective Hamiltonian formalism. Therein, a $M \times M$ Hamiltonian H_0 describes the internal system, its coupling to the N channels is characterized by a matrix V, and $S(\omega) = -iV^T[\omega - H_0 + i(VV^T + \Gamma_a)/2]^{-1}V$ [18, 19, 20]. The scattering matrix can also be decomposed in terms of the system's natural resonances (the poles) as [18, 21, 22]

$$S(\omega) = -i\Sigma_{m=1}^{M} \frac{W_m W_m^T}{\omega - \omega_m + i(\Gamma_m + \Gamma_a)/2}. \tag{1}$$

The complex eigenfrequencies $\omega_m = \omega_m - i\Gamma_m/2$ are the eigenvalues of the effective Hamiltonian $H_{eff} =$

$H_0 - iVV^T/2$ and the modal vectors W_m are the projections of the eigenfunctions ϕ_m of H_{eff} onto the channels: $W_m = V^T\phi_m$. Using the completeness of the eigenfunctions, it can be demonstrated (see SI) that the eigenstate corresponding to a CPA condition at $\omega = \omega_n$, $S(\omega_n)\psi_{CPA} = 0$, is the time-reverse of the modal wavefront: $\psi_{CPA} = W_n^*/\|W_n\|$. ψ_{CPA} hence provides maximal excitation of the selected mode [22, 23]. The interpretation of W_n^* as the time-reversed output of a lasing mode (if loss mechanisms were replaced by gain mechanisms of equal strength) led to the term "anti-laser" [3, 7, 12], an analogy that should be used with caution since it neglects essential nonlinear processes in laser operation.

Any realistic experimental observation of CPA is however inevitably confronted with multiple practical imperfections: (i) noise corrupts the measurement of S such that one measures $S + \Delta S$, (ii) a small mismatch $\Delta\Gamma$ between the modal linewidth and losses: $\Gamma_a = \Gamma_n + \Delta\Gamma$, (iii) a frequency shift $\Delta\omega = \omega - \omega_n$. In the vicinity of the CPA condition, the resonance associated with the real-valued zero dominates the sum in Eq. (1). The latter implies that ψ_{CPA} is still an eigenvector of S with a reflection coefficient which is therefore not zero but (see SI for algebraic details)

$$R(\omega) = \frac{4\Delta\omega^2 + (\Delta\Gamma)^2}{4\Delta\omega^2 + (2\Gamma_n + \Delta\Gamma)^2} + \frac{\|\Delta S\|_F^2}{N}. \tag{2}$$

We will show below that this equation explains the characteristic shape of the reflection dip and can be exploited to extract the experimental parameters by fitting the measured data with this model.

2.2 Time Delay

Having an analytical description of the reflection dip at the CPA condition in a random system, we can move on to study the associated time delays. Various metrics to quantify time delays have been put forth in the literature, usually oblivious to the impinging wavefront [24, 25, 26]. In contrast, here we are interested in the delay of the signal that exits the system without being absorbed if we inject the CPA wavefront. Thus we define the time delay of a specific incoming wavefront ψ_{in} that is scattered in our multichannel system via the Wigner-Smith operator $Q(\omega) = -iS(\omega)^\dagger\partial_\omega S(\omega)$ which involves the derivative of $S(\omega)$ with angular frequency:

$$\tau(\omega) = \frac{\psi_{in}^\dagger Q(\omega)\psi_{in}}{\psi_{in}^\dagger S(\omega)^\dagger S(\omega)\psi_{in}}. \tag{3}$$

The real part of the complex-valued $\tau(\omega)$ is related to the frequency derivative of the scattering phase and can hence be interpreted as the delay of reflected intensity for an incoming pulse with vanishing bandwidth. The imaginary part of $\tau(\omega)$ is related to the variation of reflected intensity with frequency [27, 28, 29]. Our model also allows us to estimate the real and imaginary parts of $\tau(\omega)$ at the CPA condition, $\psi_{in} = \psi_{CPA}$, (see SI):

$$Re[\tau(\omega)] = \frac{1}{R(\omega)} \frac{4\Gamma_n(4\Delta\omega^2 - \Delta\Gamma(2\Gamma_n + \Delta\Gamma))}{[4\Delta\omega^2 + (2\Gamma_n + \Delta\Gamma)^2]^2} \tag{4}$$

and

$$Im[\tau] = -\frac{4\Gamma_n}{4\Delta\omega^2 + \Delta\Gamma^2} \frac{4\Delta\omega(\Gamma_n + \Delta\Gamma)}{4\Delta\omega^2 + (2\Gamma_n + \Delta\Gamma)^2}, \tag{5}$$

where $R(\omega)$ is given by Eq. (2). Obviously both the real and imaginary parts of $\tau(\omega)$ diverge as $\Delta\omega \to 0$ and $\Delta\Gamma \to 0$, which confirms the intuition that the wave injected into the system is trapped for an infinitely long time at the CPA condition.

Surprisingly, we observe a phase transition of $Re[\tau(\omega = \omega_n)]$ as the amount of losses increases and surpasses the modal linewidth. When the zero $z_n = \omega_n + i(\Gamma_n - \Gamma_a)/2$ is located in the upper half of the complex frequency plane ($\Gamma_a < \Gamma_n$), the time delay $Re[\tau(\omega)]$ is positive. At the crossover of the real

frequency axis ($\Gamma_a = \Gamma_n$), a singularity occurs and $|Re[\tau(\omega)]|$ diverges. When losses dominate the coupling to channels, $\Gamma_a > \Gamma_n$, $Re[\tau(\omega)]$ becomes negative. We note here that negative time delays have previously been found for wavefronts that are strongly absorbed by lossy resonant targets within multiply scattering media [30, 31, 29] and transmission through diffusive random media [25, 26]. Negative time delays arise due to the distortion of the incident pulse for which the intensity is more strongly absorbed at long lifetimes than at early times (see SI).

2.3 Sensitivity to Perturbations

We now seek to demonstrate that the strong enhancement of the delay time provides an extreme sensitivity of the outgoing field to tiny perturbations within the system. To establish this link, let us begin by considering the *generalized* Wigner-Smith operator $Q_\alpha = -iS^\dagger \partial_\alpha S$ [32] defined with respect to a change of a parameter α of the system; α can be a local or a global parameter. In systems where S is close to unitarity, the optimal eigenstates of Q_α provide the optimal wavefronts to locally manipulate a perturber [32, 33]. In analogy with the delay time in Eq. (3), the variations of the outgoing field for a change of α are encapuslated within the complex parameter $\tau_\alpha = \psi_{in}^\dagger Q_\alpha \psi_{in}/R$. The relation between the delay time $\tau(\omega)$ and τ_α at the CPA condition can be established using the modification of the system's resonances due to the perturbation.

First, we note that upon injection of the CPA wavefront ($\psi_{in} = \psi_{CPA}$), the variation of the outgoing field in the vicinity of the CPA condition results from the change of a single eigenstate (labelled n) in Eq. (1). This property yields a linear relation between the projection of the CPA wavefront on Q_α and on the *generalized* Wigner-Smith operator applied to a perturbation of ω_n, $Q_{\omega_n} = -iS^\dagger \partial_{\omega_n} S$,

$$\psi_{CPA}^\dagger Q_\alpha \psi_{CPA} = [\partial_\alpha \omega_n] \psi_{CPA}^\dagger Q_{\omega_n} \psi_{CPA}. \tag{6}$$

The perturbation-induced shift in ω_n is given by $\partial_\alpha \omega_n = \beta \nabla |\phi(r)|^2$ for local perturbations, where $\nabla |\phi(r)|^2$ is the gradient of the energy density taken in the direction of the displacement and β depends on the geometry of the perturber [34].

Second, in the approximation of a single resonance contribution, the projection on the operators $Q = -iS^\dagger \partial_\omega S$ and Q_{ω_n} yields the same result except for a global minus sign. This provides the sought-after relation between $\tau(\omega)$ and τ_α for the CPA condition:

$$\tau_\alpha = -[\partial_\alpha \omega_n] \tau(\omega). \tag{7}$$

The divergence of $\tau(\omega)$ hence leads to an extreme sensitivity of the outgoing field. In our case, the CPA wavefront does not provide focusing on a perturber but is the optimal wavefront to detect a tiny variation anywhere within the cavity. We emphasize that ψ_{CPA} is also the optimal eigenvector of the operator $-iS^{-1}\partial_\alpha S$ (see SI). This property results from the vanishing eigenvalue of S leading to a pseudo-inverse matrix S^{-1} dominated by a single eigenstate.

Equation (7) directly provides the sensitivity of the reflection coefficient at the CPA condition. Using that $\partial_\alpha R = -2Im[\psi_{CPA}^\dagger Q_\alpha \psi_{CPA}]$, we obtain

$$\frac{1}{R}\partial_\alpha R = [\partial_\alpha \omega_n] Im[\tau(\omega)]. \tag{8}$$

The derivative of the logarithm of the reflection coefficient ($\partial_\alpha log(R) = [\partial_\alpha R]/R$) hence increases extremely rapidly in the vicinity of the CPA condition. This unique feature makes it possible to finely characterize the strength of the perturbation from the shape of the reflection dip. Because the change in R is proportional to the change in ω_n, this dip is anew given by Eq. (2) in which $\Delta\omega$ has to be replaced with $\Delta\omega_n \sim \Delta\alpha[\partial_\alpha \omega_n] = \Delta\alpha[\beta \nabla |\phi(r)|^2]$.

We note that another slightly different operator has been introduced in recent related work to maximize the measurement precision of an observable parameter [35]. The eigenstates of the operator $F_\alpha = (\partial_\alpha S)^\dagger \partial_\alpha S$ have indeed been identified as "maximum information states" maximizing the Fisher-information related to the parameter α. F_α coincides with Q_α only for a unitary scattering matrix. The results in

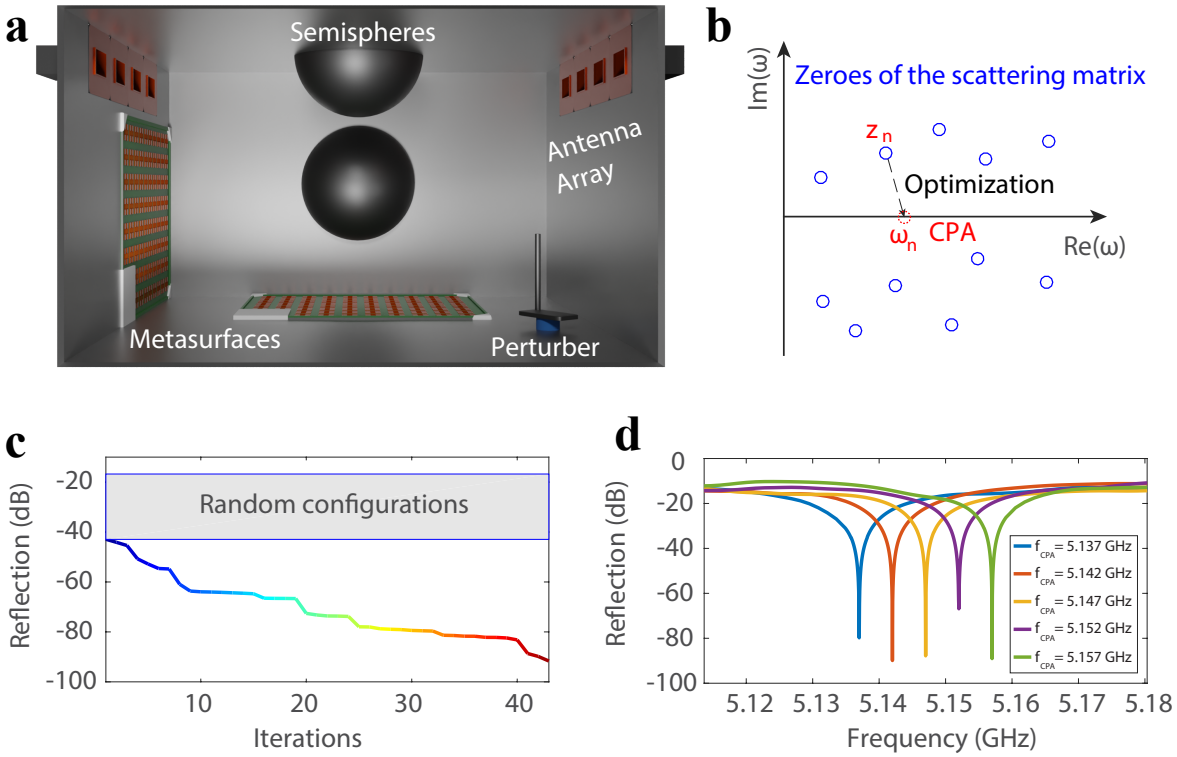

Figure 1: **"On-demand" realization of CPA in a programmable complex scattering enclosure. a,** Experimental setup consisting of a three-dimensional electrically large irregular metallic enclosure equipped with two arrays of 1-bit reflection-programmable meta-atoms to tune the system's scattering properties. The system is connected to eight channels via waveguide-to-coax transitions. Small perturbations of the system can be induced by rotating a metallic rod placed on a metallic platform. **b,** Illustration of operation principle in the complex frequency plane. By tuning the system's scattering properties with the programmable meta-atoms, a zero of the scattering matrix is moved onto the real frequency axis at a target horizontal position (here 5.147 GHz). **c,** Dynamics of an example iterative optimization of the meta-atom configurations. **d,** Spectrum of the multi-channel reflection coefficient $R(\omega)$ for five optimized systems targeting five distinct regularly spaced nearby target frequencies between 5.137 GHz and 5.157 GHz.

Ref. [35] however differ sharply from our present work in three important ways: first, while Ref. [35] considers a "random" configuration of a disordered medium, we operate under the very special CPA condition for which S has a real-valued zero; second, while Ref. [35] identifies a so-called "maximum information state" that is specific to the observable of interest (e.g. location of the pertuber), our CPA condition yields an optimal sensitivity to *any* perturbation irrespective of its location; third, the approach of Ref. [35] requires perturbations of the specific variable of interest in order to determine the input wavefront.

3 Experimental Measurement of Time Delays

Having established a theoretical model for the characteristic reflection dip and delay time associated with CPA, we now seek to verify its validity in experiments. Experimentally realizing CPA in a random medium is a very challenging task that was only mastered recently for the first time [12, 13]. These early realizations relied on both ω and Γ_a being freely tunable parameters to identify a setting in which one zero of $S(\omega)$ lies on the real frequency axis. For our experiments, we consider a more realistic three-dimensional complex scattering enclosure with fixed homogeneously distributed losses and we fix the working frequency to 5.147 GHz. In order to realize CPA "on demand" without control over ω and Γ_a, we dope our system with reflection-programmable meta-atoms (see Experimental Section). In our experiment illustrated in Figure 1a and as detailed in the Experimental Section, $N = 8$ channels are connected to a chaotic cavity and an iterative algorithm is used to optimize the configuration of the 304 meta-atoms.

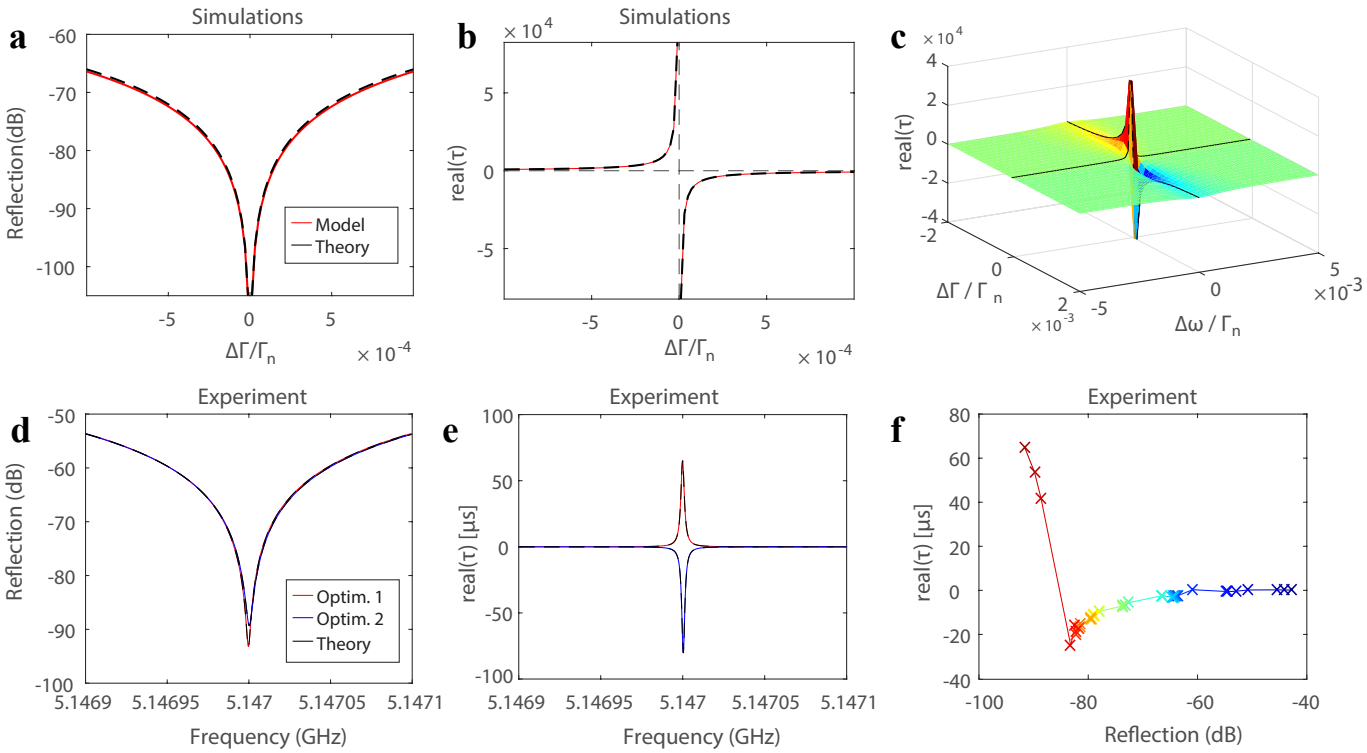

Figure 2: **CPA signature on time delays.** Multichannel reflection coefficient $R(\omega)$ (**a**) and time delay $Re[\tau(\omega)]$ (**b**) found in random matrix simulations with an effective Hamiltonian model (red lines) in the vicinity of a CPA condition at ω_n for a mode with linewidth Γ_n, plotted as a function of linewidth detuning $\Delta\Gamma/\Gamma_n = (\Gamma_a - \Gamma_n)/\Gamma_n$. The time delay has been normalized by its value in absence of absorption. These numerical results are in excellent agreement with our theoretical predictions (black dashed lines) given by Eq. (2) and Eq. (4). **c,** Variations of the time delay with $\Delta\Gamma/\Gamma_n$ and frequency detuning $\Delta\omega/\Gamma_n = (\omega - \omega_n)/\Gamma_n$ are visualized as three-dimensional surface. The experimental results in **d** and **e** as a function of frequency detuning are also perfectly fitted with our theory for two different realizations of the CPA condition. **f,** Evolution of time delay during an example optimization. The absolute time delay $|Re[\tau(\omega)]|$ increases as $R(\omega_0)$ is minimized but the sign of $Re[\tau(\omega)]$ jumps from negative to positive after 40 iterations. This is a signature of the time-delay singularity. The color-code indicating the iteration index is the same as in Figure 1c.

The latter allow us to tweak S such that one of its zeros hits the real frequency axis [17], as illustrated schematically in Figure 1b. This approach generalizes the technique of purposefully perturbing a random scattering enclosure to achieve perfect absorption presented in Ref. [17] from single-channel excitation to multi-channel excitation. Moreover, our setup includes an irregular metallic structure attached to a rotation stage; we can thus identify different realizations of CPA by rotating this "mode-stirrer" to different positions and optimizing the meta-atom configurations for each position.
Random configurations of the meta-atoms yield reflection values between -20 dB and -40 dB. Starting from a configuration corresponding to roughly -40 dB, our optimization algorithm which minimizes the reflection $R = \|S\psi_{in}\|^2$ eventually identifies a setting with $R \sim 4.85 \times 10^{-10} = -93$ dB, as depicted in Figure 1c. We then repeat the experiment for other predefined frequencies. In each case, the corresponding reflection spectrum in Figure 1d displays the expected very narrow and deep dip at the desired working frequency.
We can now test our theoretical model's prediction for the reflection and delay time at the CPA condition. Before confronting it with our experimental data, we perform a random matrix simulation for which the internal Hamiltonian H_0 is a a real symmetric matrix drawn from the Gaussian orthogonal ensemble and V is a real random matrix with Gaussian distribution [36]. We select a resonance and explore the variations of $R(\omega)$ and $Re[\tau(\omega)]$ near the CPA condition as a function of the normalized linewidth mismatch $\Delta\Gamma/\Gamma_n$ and frequency detuning $\Delta\omega/\Gamma_n$. As shown in Figure 2a-c, the dip in the reflection coefficient and the singularity of the time delay found in simulations are perfectly reproduced by Eqs. (2) and (4). In particular, Figure 2b highlights the divergence of $Re[\tau(\omega)]$ as $\Delta\Gamma \to 0$ with positive (negative) values when the zero lies in the upper (lower) complex plane.
To compare our theoretical model with our experiment, we extract the parameters involved in the model, that is Γ_n, $\Delta\Gamma$ and $\|\Delta S\|_F^2$, by fitting our model to the spectra of $R(\omega)$ and $Re[\tau(\omega)]$. We thereby obtain a linewidth $\gamma_{CPA} = \Gamma_{CPA}/(2\pi) \sim 51$ MHz, a mismatch $\Delta\Gamma/(2\pi) \sim 1.3$ kHz and a relative noise level $\|\Delta S\|_F^2/\|S\|_F^2 \sim 3 \times 10^{-9}$. As seen in Figure 2d,e, our model exactly fits our experimental data on a frequency range smaller than the mean level spacing $\Delta = \langle\omega_{n+1} - \omega_n\rangle/(2\pi)$ given by Weyl's law, $\Delta = c_0^3/(8\pi V f^2) \sim 0.54$ MHz. The very small value of $\Delta\Gamma$ evidences that our optimized system is extremely close to the CPA condition. In Figure 2e we observe a strong enhancement of the time delay for two representative realizations of CPA; $|Re[\tau(\omega)]|$ reaches values as high as 80 μs. For comparison, wavefronts that are orthogonal to ψ_{CPA} yield an average time delay of 10.9 ns, almost four orders of magnitude smaller. The two CPA realizations in Figure 2d,e associated with a positive (negative) time delay correspond to a zero of S just above (below) the real frequency axis. During the optimization of the meta-atom configurations, the zero can even cross the real frequency axis, an example thereof being shown in Figure 2f for which $Re[\tau(\omega)]$ suddenly jumps from -25 μs to 41 μs after a single iteration.

4 Time Delay Singularity for Optimal Sensitivity

Now that we have have established and experimentally confirmed the physical origin of the time-delay singularity at the CPA condition in complex scattering media, we go on to investigate experimentally how this singularity can enhance the sensitivity of measurements to parametric perturbations, which is essential in sensing applications. The term "sensitivity" in the present work refers to a transduction coefficient of the sensor from the quantity to be measured (a perturbation $\Delta\alpha$ of a parameter α) to an intermediate output quantity. This should not be confused with the smallest measurable change of the input quantity which pivotally depends on the measurement noise [37]. In the following, first, we show that at the CPA condition, the ability to detect tiny perturbations is enhanced due to a rapid field decorrelation, the latter being intimately linked to the time delay. Then, second, we investigate the extent to which the CPA condition also enables a characterization of the perturbation in terms of its strength.
Wave chaos is generally known to be quite sensitive to perturbations; techniques known as diffuse wave spectroscopy (DWS) study the decorrelation of the outgoing field due to a dynamic perturbation in order to quantify the latter [38, 39, 40] and "reverberation coded apertures" enable deeply sub-wavelength object localization [41]. These techniques benefit from ergodicity which ensures that the sensitivity to

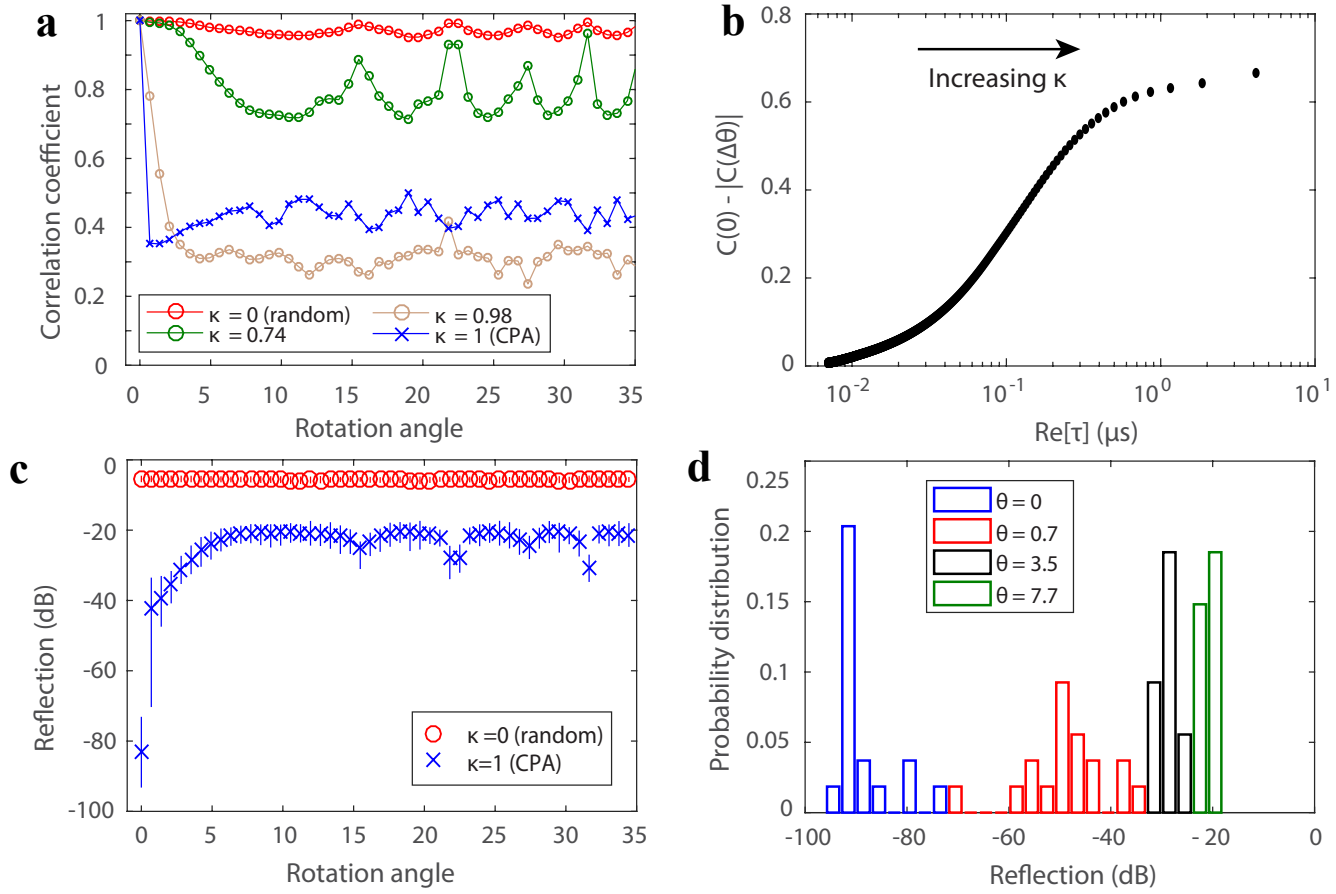

Figure 3: **Enhanced sensing with the time-delay singularity at the CPA condition. a,** Magnitude of the correlation coefficient $C(\psi_{in}, \theta)$ of the outgoing field as a function of the size of the perturbation (angle of rotation θ) for $\kappa = 0$ (fully random wavefront), $\kappa = 0.74$, $\kappa = 0.98$ and $\kappa = 1$ (CPA wavefront). **b,** Decorrelation rate $C(0) - |C(\Delta\theta)|$ as a function of the delay time for incoming wavefronts with κ increasing from 0 to unity. **c,** Multichannel reflection coefficient for $\kappa = 0$ and $\kappa = 1$. **d,** Histogram of observed reflection values for different perturbation strengths, based on 18 CPA realizations with different initial orientations of the perturber.

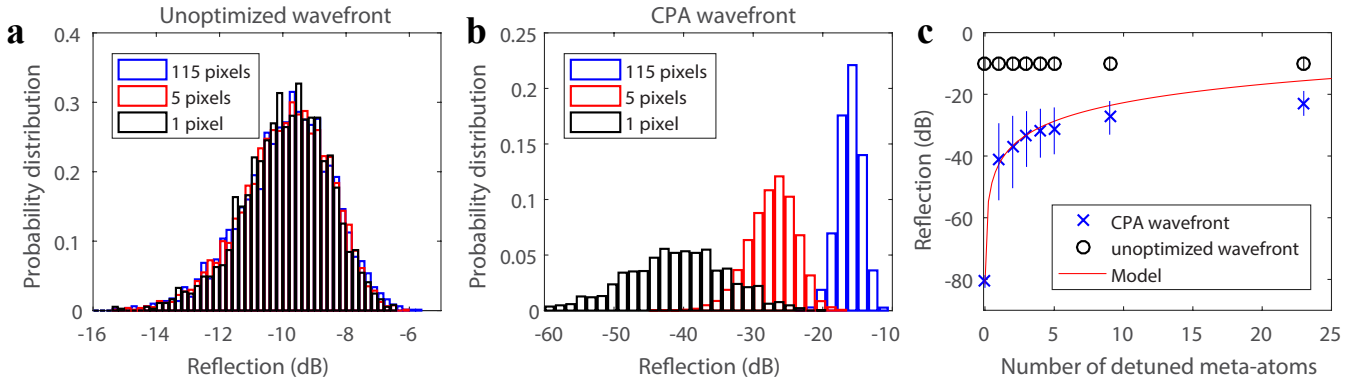

Figure 4: **Sensing the perturbation strength of detuned meta-atoms. a, b,** Distributions of R shown for a random incoming wavefront (**a**) and the CPA wavefront (**b**) for detuning 1, 5 and 115 meta-atoms. **c,** Variations of the reflection coefficient on a logarithmic scale at the CPA condition (blue crosses) and for a random incoming wavefront (black circles), as a function of the number of detuned meta-atoms p. The bars give the corresponding 90 percentiles for R. For small perturbations, the result obtained with the CPA wavefront is well explained by Eq. (2) upon substituting $\Delta\omega = 2\pi K p$, with $K = 0.35$ MHz (see main text for details).

perturbations (determined by the dwell time) has statistically similar properties throughout the system and for different realizations of the system. In contrast, here we are interested in the sensitivity to small perturbations of a system in one specific state. Purely relying on the sensitivity of wave chaos corresponds (in our system tuned to have a real-valued zero) to injecting an unoptimized random wavefront $\psi_{in} = \psi_{rand}$. However, because of the divergence of the delay time, the perturbation-induced decorrelation of the wave may be dramatically enhanced by injecting the optimized wavefront $\psi_{in} = \psi_{CPA}$. We begin by defining a correlation coefficient based on the outgoing field as

$$C(\Delta\alpha, \psi_{in}) = \frac{\psi_{out}^{\dagger}(\alpha + \Delta\alpha)\psi_{out}(\alpha)}{\sqrt{R(\alpha)R(\alpha + \Delta\alpha)}}. \quad (9)$$

To confirm the predicted rapid decorrelation of the outgoing field at the CPA condition experimentally, we gradually perturb the system by rotating a small metallic structure (a metallic pillar located on a metallic platform, see Figure 1a) in steps of $\Delta\theta = 0.62°$ (see Figure 3a). At each step, we measure $S(\theta)$ and evaluate the outgoing field $\psi_{out}(\theta) = S(\theta)\psi_{in}$ for wavefronts defined as $\psi_{in}(\kappa) = \kappa\psi_{CPA} + (1-\kappa)\psi_{rand}$ and normalized to unity. $\psi_{in}(\kappa = 0)$ is hence an unoptimized wavefront while $\psi_{in}(\kappa = 1)$ yields the CPA wavefront. We repeat this procedure for 18 realizations of different initial positions of the rotating object. In Figure 3a we plot $|C(\Delta\alpha = \theta)|$ as a function of the size of the perturbation (here the angle of rotation θ).

For $\psi_{in} = \psi_{rand}$, the field barely decorrelates even after 100 rotation steps. In other words, DWS-based sensing would not be capable of detecting or quantifying the perturbation that we consider. In contrast, for $\psi_{in} = \psi_{CPA}$, the field strongly decorrelates even for the smallest step. Figure 3a therefore evidences the extreme sensitivity of the CPA condition for precision sensing in complex systems, well beyond that achievable with traditional DWS. The link between the enhancement of the sensitivity and the enhancement of the delay time near the CPA condition is confirmed in Figure 3b. For different values of κ between zero and unity, we evaluate both the corresponding decorrelation rate $C(0) - |C(\Delta\theta)|$ for the smallest rotation step $\Delta\theta$ and the corresponding time delay $Re[\tau]$. The resulting plot in Figure 3b evidences the dramatic increase of $C(0) - |C(\Delta\theta)|$ as $Re[\tau]$ increases. $C(0) - |C(\Delta\theta)|$ reaches a plateau for very large delay times as the smallest step is larger than the rotation giving a complete decorrelation of the outgoing field.

Having clarified that the rapid decorrelation of the outgoing field enhances the ability to detect the presence of a perturbation, we now explore to what extent this perturbation can also be characterized. For a chaotic cavity (not tuned to have a real-valued zero) and/or a random incoming wavefront, the average reflection coefficient is statistically independent of the perturbation strength. In contrast, at the CPA condition, $R(\alpha + \Delta\alpha)$ increases with $\Delta\alpha$ so that it may be possible to discriminate between two perturbations $\Delta\alpha_1$ and $\Delta\alpha_2$ based on measurements of $R(\Delta\alpha_1)$ and $R(\Delta\alpha_2)$. The reflection coefficient $R(\theta, \psi_{CPA})$ shown in Figure 3c increases rapidly with θ but then saturates for $\theta > 5°$. Note that the plateau reached for large angles is 20 dB below $R(\theta, \psi_{rand})$ because the perturbation is small.

In wave-chaotic systems as our complex scattering enclosure, the energy density (and hence $\partial_\alpha\omega_n$ and R) are distributed quantities which fluctuate for different realizations of the system; an example are the histograms of $R(\theta, \psi_{CPA})$ shown in Figure 3d. To investigate the dependence of $R(\alpha + \Delta\alpha)$ on the perturbation strength $\Delta\alpha$, a statistical analysis is hence required. We conveniently achieve this in Figure 4 by considering a different type of perturbation: the detuning of p meta-atoms away from the CPA configuration [17]. We successively determine R for 200 realizations of p detuned meta-atoms in 15 CPA realizations, with p varying from $p = 1$ to $p = 115$.

As expected, for random wavefronts, $R(p, \psi_{rand})$ is statistically independent of p: the distributions $P(R(p, \psi_{rand})$ found for $p = 1$, 5 and 115 detuned meta-atoms hence completely overlap, as seen in Figure 4a. In contrast, Figure 4b reveals that $P(R(p, \psi_{CPA}))$ strongly depends on p because the variations of ω_n due to local changes of the boundary conditions increase with the number of detuned meta-atoms. We find that in the regime of small perturbations (here $p \leq 5$), $\langle R(p, \psi_{CPA})\rangle$ is in good agreement with Eq. (2) upon replacing the frequency shift $\Delta\omega = \omega - \omega_n$ with $2\pi Kp$, where $K = 0.35$ MHz is a constant depending on the scattering cross-section of the meta-atoms and the volume of the cavity. Our model's validity is

confirmed by its faithful fit to the experimental data for $p \leq 5$ in Figure 4c.
Nonetheless, we point out that R being a distributed quantity results in fundamental limits on the precision with which the strength of any given perturbation can be determined. Indeed, the distributions $P(R(p, \psi_{CPA}))$ partially overlap for close values of p, as shown in Figure 4b. This limitation may be understood as the price for the enhanced sensitivity to any perturbation within the system irrespective of its location.

5 Discussion

The discussed CPA condition can be interpreted as a special case of two distinct more general scattering phenomena: coherently enhanced absorption (CEA, [42]) and virtual perfect absorption (VPA, [43]).
CEA is a route to achieving very low (but finite) reflection values over an extended frequency range. Similarly to CPA, CEA relies on injecting the incoming wavefront giving the smallest reflection, which is the eigenstate of the matrix $S^\dagger(\omega)S(\omega)$ with minimal eigenvalue. Unless a zero of S happens to lie on the real-frequency axis at ω, this eigenstate generally does not correspond to an eigenstate of S (CPA condition) so that the reflection coefficient does not vanish. Multiple resonances of the system are then involved and the reflection dip associated with CEA is not as pronounced as for CPA. In the case of CEA, the reflection coefficient decorrelates on a scale inversely proportional to the absorption mean free path [42]. The time delay of waves and the sensitivity of the medium to a perturbation are hence generally bounded for CEA.
The idea of CPA is to bring a zero onto the real-frequency axis such that it can be accessed with a monochromatic excitation oscillating at a real frequency. If, however, the zero is not on the real frequency axis, it can still be accessed in the transient regime using a nonmonochromatic signal oscillating at a complex frequency. This VPA concept was recently studied for regular (almost) lossless systems for which the zero always lies in the upper half of the complex frequency plane [43, 44]. Consequently, the excitation signal has to exponentially increase in time to interfere destructively with the waves reflected off the system. The interaction of the incident pulse with the scattering medium then provides ideal energy storage until the interruption of the exponential growth of the injected signal. Given the generality of the scattering matrix formalism, this concept can be extended to disordered lossy matter such as complex scattering enclosures. The zeros may then lie anywhere in the complex frequency plane, implying that the necessary excitation is not always an exponentially increasing one. Interesting links with the sign of the time delay as discussed in the present work then arise.
To summarize, we have proposed a theoretical description of the hallmark sign of CPA in complex scattering system and we verified our theory experimentally. Our work rigorously explains the divergence of the time delay at the CPA condition and how this singularity justifies the optimal sensitivity of the CPA condition for detecting minute perturbations. This feature will enable novel precision sensing tools but also impact other areas such as filter applications and secure wireless communication [17, 13]. Furthermore, our experiments demonstrated how a CPA condition can be accessed "on demand" at an arbitrary frequency without controlling the level of attenuation in the system. Finally, we note that our results are very general in nature and apply to other types of wave phenomena, too. Looking forward, it may be feasible to engineer a CPA exceptional point in a random scattering medium, requiring the coalescence of two or more real-valued zeros and the corresponding eigenvectors, which may alter the functional dependence of the reflection coefficient on various kinds of detuning [45]. Further inspiration for future work may also be found in recent papers based on regular (rather than randomly scattering) systems involving the tailoring of CPA and lasing [46, 47, 48, 49].
Note added. — In the process of finalizing this manuscript, we became aware of related work [50] that also generalizes the concept of "on-demand" access to a real-valued scattering matrix zero in a metasurface-tunable complex scattering enclosure from single-channel [17] to multi-channel excitation.
Note added. — During the peer review process of this manuscript, a preprint [51] appeared that studies the generalization of the Wigner time delay from unitary systems to sub-unitary systems with global losses and/or spatially localized loss centers. Therein, the authors point out that in the presence of lo-

calized loss mechanisms (a scenario *not* compatible with our theoretical and experimental work in which losses are uniform), the real parts of associated poles and zeros of the scattreing matrix are in general not identical.

6 EXPERIMENTAL SECTION

Experimental Setup

Our complex scattering enclosure (depicted in Figure 1a) is a metallic cuboid ($50 \times 50 \times 30\ cm^3$) with two hemispheres on the inside walls to create wave chaos. In short, the difference between the trajectories of two rays launched from the same position in slightly different directions will increase exponentially in time. The system is excited via eight antennas (waveguide-to-coax transitions designed for operation in the $4 < \nu < 7$ GHz range) which are connected to an eight-port vector network analyser (VNA). The VNA acquires the full 8×8 scattering matrix in one go. It emits signals at 0 dBm and operates with an intermediate-frequency bandwidth of 2 kHz to ensure a high signal-to-noise ratio. In the vicinity of the targeted CPA frequency $\nu_0 = 5.147$ GHz, we measure the spectra with an extremely small frequency step ($\Delta\nu = 1$ kHz) and subsequently fit them with a linear regression in the Argand diagram to further reduce the impact of noise.

In order to tune our random system's scattering matrix, two programmable metasurfaces [52] are placed on two neighboring walls of the cavity [53]. Each metasurface consists of an array of 152 1-bit programmable meta-atoms. Each meta-atom has two digitalized states, "0" and "1", with opposite electromagnetic responses. The working principle relies on the hybridization of two resonances of which one is tunable via the bias voltage of a pin diode; details can be found elsewhere [54]. The two states are designed to mimic Dirichlet and Neumann boundary conditions and their detailed characteristics are provided in the SI.

Based on the experimentally measured 8×8 scattering matrix and the linearity of the wave equation, we can precisely calculate the outgoing wavefront ψ_{out} for any desired injected wavefront ψ_{in} via $\psi_{out} = S(\omega)\psi_{in}$. To access the CPA scattering anomaly, the injected wavefront must correspond to the eigenvector of the scattering matrix associated with a zero eigenvalue. In general, for a complex scattering system the required input wavefront ψ_{CPA} looks seemingly random.

Optimization of Meta-Atom Configurations

Identifying a configuration of the programmable metasurfaces that yields CPA at the targeted frequency is a non-trivial task since there is no forward model describing the impact of the metasurface configuration on S. Hence, we opt for an iterative optimization algorithm similar to the one in Ref. [55]. We begin by measuring S for 200 random configurations. We then use the configuration for which the smallest eigenvalue λ_8 of $S(\nu_0)$ is the lowest as starting point. For each iteration, we randomly select z meta-atoms and flip their state. If the resulting $S(\nu_0)$ has a lower λ_8, we keep the change. We gradually reduce the number of meta-atoms whose state is flipped per iteration, according to $z = max(int(50e^{-0.02k}), 1)$, where k is the iteration index. As typical for inverse design problems, there is no guarantee that our optimization algorithm identifies the globally optimal configuration. However, typically it rapidly identifies a local optimum and runs with different random initializations tend to yield distinct local optima of comparable quality.

Characterization of Chaotic Cavity

We characterize our system's linewidth associated with the N attached channels, $N\gamma_c$, and its linewidth associated with global absorption effects, γ_a, in the following. To that end, we measure $S(\omega)$ for 300 random metasurface configurations and repeat the measurements for a number of channels connected to the cavity varying from $N = 3$ to $N = 8$. In each case, we estimate the average linewidth $\langle\gamma\rangle$ by fitting the exponential decay of average reflected intensities in the time domain, $I(t) = e^{-2\pi\langle\gamma\rangle t}$ (see SI for details). Using the variations of $\langle\gamma\rangle$ with respect to the number of attached channels, $\langle\gamma\rangle = \langle\gamma_a\rangle + N\langle\gamma_c\rangle$, we obtain an average absorption strength $\langle\gamma_a\rangle = 11.2$ MHz and a linewidth associated with the channels $\langle\gamma_n\rangle = 8\langle\gamma_c\rangle = 0.33$ MHz. Compared with the linewidth γ_{CPA} found at the CPA condition it appears

at first sight surprising that γ_{CPA} exceeds $\langle\gamma_a\rangle$ and $\langle\gamma_n\rangle$ by more than one order of magnitude. The apparent paradox is resolved by noting that the resonance widths in wave-chaotic systems are not normally distributed; instead they have a distribution skewed toward lower values with a long tail for larger values [56, 57]. Such a distribution is not fully characterized by its average, and observing values well above the average, as in the case of γ_{CPA}, is by no means impossible.

Supporting Information
Supporting Information is available from the Wiley Online Library or from the author.

Acknowledgements
This publication was supported by the French "Agence Nationale de la Recherche" under reference ANR-17-ASTR-0017, by the European Union through the European Regional Development Fund (ERDF), and by the French region of Brittany and Rennes Métropole through the CPER Project SOPHIE/STIC & Ondes. The metasurface prototypes were purchased from Greenerwave. The authors acknowledge P. E. Davy for the 3D rendering of the experimental setup in Figure 1a. M. D. acknowledges the Institut Universitaire de France.

Conflict of Interests
The authors declare no conflict of interests.

Author Contributions
M.D. developed the theoretical model. P.d.H. and M.D. jointly conceived and conducted the experimental work and wrote the manuscript. K.Y. assisted with the experiments. All authors discussed the results and commented on the manuscript.

References

[1] A. Krasnok, D. Baranov, H. Li, M.-A. Miri, F. Monticone, A. Alú, *Adv. Opt. Photon.* **2019**, *11*, 4 892.

[2] V. Grigoriev, A. Tahri, S. Varault, B. Rolly, B. Stout, J. Wenger, N. Bonod, *Phys. Rev. A* **2013**, *88*, 1 011803.

[3] Y. Chong, L. Ge, H. Cao, A. D. Stone, *Phys. Rev. Lett.* **2010**, *105*, 5 053901.

[4] D. G. Baranov, A. Krasnok, T. Shegai, A. Alù, Y. Chong, *Nat. Rev. Mater.* **2017**, *2*, 12 17064.

[5] M. Cai, O. Painter, K. J. Vahala, *Phys. Rev. Lett.* **2000**, *85*, 1 74.

[6] W. Wan, Y. Chong, L. Ge, H. Noh, A. D. Stone, H. Cao, *Science* **2011**, *331*, 6019 889.

[7] Z. J. Wong, Y.-L. Xu, J. Kim, K. O'Brien, Y. Wang, L. Feng, X. Zhang, *Nat. Photon.* **2016**, *10*, 12 796.

[8] H. Cao, *Waves Random Media* **2003**, *13*, 3 R1.

[9] D. S. Wiersma, *Nat. Phys.* **2008**, *4*, 5 359.

[10] Y. V. Fyodorov, S. Suwunnarat, T. Kottos, *J. Phys. A* **2017**, *50*, 30 30LT01.

[11] H. Li, S. Suwunnarat, R. Fleischmann, H. Schanz, T. Kottos, *Phys. Rev. Lett.* **2017**, *118*, 4 044101.

[12] K. Pichler, M. Kühmayer, J. Böhm, A. Brandstötter, P. Ambichl, U. Kuhl, S. Rotter, *Nature* **2019**, *567*, 7748 351.

[13] L. Chen, T. Kottos, S. M. Anlage, *Nat. Commun.* **2020**, *11* 5826.

[14] J. Zhang, K. F. MacDonald, N. I. Zheludev, *Light Sci. Appl.* **2012**, *1*, 7 e18.

[15] R. Bruck, O. L. Muskens, *Opt. Express* **2013**, *21*, 23 27652.

[16] S. M. Rao, J. J. Heitz, T. Roger, N. Westerberg, D. Faccio, *Opt. Lett.* **2014**, *39*, 18 5345.

[17] M. F. Imani, D. R. Smith, P. del Hougne, *Adv. Funct. Mater.* **2020**, *30* 2005310.

[18] I. Rotter, *Phys. Rev. E* **2001**, *64*, 3 036213.

[19] Y. V. Fyodorov, D. Savin, H. Sommers, *J. Phys. A* **2005**, *38*, 49 10731.

[20] I. Rotter, *J. Phys. A* **2009**, *42*, 15 153001.

[21] F. Alpeggiani, N. Parappurath, E. Verhagen, L. Kuipers, *Phys. Rev. X* **2017**, *7*, 2 021035.

[22] M. Davy, A. Z. Genack, *Nat. Commun.* **2018**, *9*, 1 4714.

[23] P. del Hougne, R. Sobry, O. Legrand, F. Mortessagne, U. Kuhl, M. Davy, *Laser Photonics Rev. TBA* 2000335.

[24] B. Van Tiggelen, P. Sebbah, M. Stoytchev, A. Genack, *Phys. Rev. E* **1999**, *59*, 6 7166.

[25] P. Sebbah, O. Legrand, A. Genack, *Phys. Rev. E* **1999**, *59*, 2 2406.

[26] A. Genack, P. Sebbah, M. Stoytchev, B. Van Tiggelen, *Phys. Rev. Lett.* **1999**, *82*, 4 715.

[27] J. Böhm, A. Brandstötter, P. Ambichl, S. Rotter, U. Kuhl, *Phys. Rev. A* **2018**, *97*, 2 021801.

[28] S. Fan, J. M. Kahn, *Opt. Lett.* **2005**, *30*, 2 135.

[29] M. Durand, S. M. Popoff, R. Carminati, A. Goetschy, *Phys. Rev. Lett.* **2019**, *123*, 24 243901.

[30] J. Muga, J. Palao, *Ann. Phys.* **1998**, *7*, 7-8 671.

[31] H. Tanaka, H. Niwa, K. Hayami, S. Furue, K. Nakayama, T. Kohmoto, M. Kunitomo, Y. Fukuda, *Phys. Rev. A* **2003**, *68*, 5 053801.

[32] P. Ambichl, A. Brandstötter, J. Böhm, M. Kühmayer, U. Kuhl, S. Rotter, *Phys. Rev. Lett.* **2017**, *119*, 3 033903.

[33] M. Horodynski, M. Kühmayer, A. Brandstötter, K. Pichler, Y. V. Fyodorov, U. Kuhl, S. Rotter, *Nat. Photonics* **2019**, 1–5.

[34] M. Barth, U. Kuhl, H.-J. Stöckmann, *Phys. Rev. Lett.* **1999**, *82*, 10 2026.

[35] D. Bouchet, S. Rotter, A. P. Mosk, *Nat. Phys.* **2021**, 1–5.

[36] U. Kuhl, O. Legrand, F. Mortessagne, *Fortschr. Phys.* **2013**, *61*, 2-3 404.

[37] W. Langbein, *Phys. Rev. A* **2018**, *98*, 2 023805.

[38] D. Pine, D. Weitz, P. Chaikin, E. Herbolzheimer, *Phys. Rev. Lett.* **1988**, *60*, 12 1134.

[39] G. Maret, *Curr. Opin. Colloid Interface Sci.* **1997**, *2*, 3 251.

[40] J. de Rosny, P. Roux, M. Fink, J. Page, *Phys. Rev. Lett.* **2003**, *90*, 9 094302.

[41] M. del Hougne, S. Gigan, P. del Hougne, *arXiv preprint arXiv:2102.05642* **2021**.

[42] Y. D. Chong, A. D. Stone, *Phys. Rev. Lett.* **2011**, *107*, 16 163901.

[43] D. G. Baranov, A. Krasnok, A. Alù, *Optica* **2017**, *4*, 12 1457.

[44] G. Trainiti, Y. Ra'di, M. Ruzzene, A. Alù, *Sci. Adv.* **2019**, *5*, 8 eaaw3255.

[45] W. R. Sweeney, C. W. Hsu, S. Rotter, A. D. Stone, *Phys. Rev. Lett.* **2019**, *122*, 9 093901.

[46] P. Bai, Y. Wu, Y. Lai, *EPL* **2016**, *114*, 2 28003.

[47] P. Bai, K. Ding, G. Wang, J. Luo, Z.-Q. Zhang, C. T. Chan, Y. Wu, Y. Lai, *Phys. Rev. A* **2016**, *94*, 6 063841.

[48] J. Luo, B. Liu, Z. H. Hang, Y. Lai, *Laser Photonics Rev.* **2018**, *12*, 8 1800001.

[49] P. Bai, J. Luo, H. Chu, W. Lu, L. Yun, *Opt. Lett.* **2020**, *45*, 24 6635.

[50] B. W. Frazier, T. M. Antonsen Jr, S. M. Anlage, E. Ott, *Phys. Rev. Res.* **2020**, *2*, 4 043422.

[51] L. Chen, S. M. Anlage, Y. V. Fyodorov, *arXiv preprint arXiv:2101.08335* **2021**.

[52] T. J. Cui, M. Q. Qi, X. Wan, J. Zhao, Q. Cheng, *Light Sci. Appl.* **2014**, *3*, 10 e218.

[53] M. Dupré, P. del Hougne, M. Fink, F. Lemoult, G. Lerosey, *Phys. Rev. Lett.* **2015**, *115*, 1 017701.

[54] N. Kaina, M. Dupré, M. Fink, G. Lerosey, *Opt. Express* **2014**, *22*, 16 18881.

[55] P. del Hougne, M. Davy, U. Kuhl, *Phys. Rev. Applied* **2020**, *13*, 4 041004.

[56] T. Kottos, *J. Phys. A* **2005**, *38*, 49 10761.

[57] U. Kuhl, R. Höhmann, J. Main, H.-J. Stöckmann, *Phys. Rev. Lett.* **2008**, *100*, 25 254101.

Table of Contents

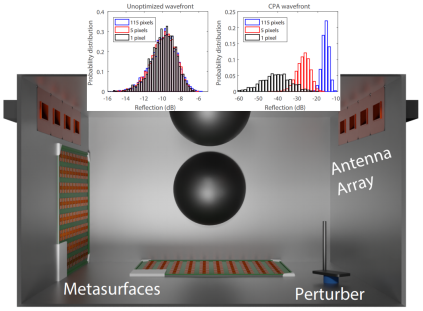

A theoretical link between the coherent perfect absorption (CPA) scattering anomaly in chaotic cavities, the associated time delay divergence and the resulting optimal sensitivity to minute arbitrary perturbations of the system is established. The results are confirmed in microwave experiments implementing eight-channel CPA in a chaotic cavity "on demand" at an arbitrary frequency by tuning the cavity's scattering properties with programmable meta-atom inclusions.